Paper

Investigation of Vehicular S-LSTM NOMA Over Time Selective Nakagami-m Fading with Imperfect CSI

Ravi Shankar[1], Bhanu Pratap Chaudhary[2], and Ritesh Kumar Mishra[2]

[1]*Electronics and Communication Engineering Department, SR University, India,*
[2]*Electronics and Communication Engineering Department, National Institute of Technology Patna, India*

https://doi.org/10.26636/jtit.2022.165722

Abstract — In this paper, the performance of a deep learning-based multiple-input multiple-output (MIMO) non-orthogonal multiple access (NOMA) system is investigated for 5G radio communication networks. We consider independent and identically distributed (i.i.d.) Nakagami-m fading links to prove that when using MIMO with the NOMA system, the outage probability (OP) and end-to-end symbol error rate (SER) improve, even in the presence of imperfect channel state information (CSI) and successive interference cancellation (SIC) errors. Furthermore, the stacked long short-term memory (S-LSTM) algorithm is employed to improve the system's performance, even under time-selective channel conditions and in the presence of terminal's mobility. For vehicular NOMA networks, OP, SER, and ergodic sum rate have been formulated. Simulations show that an S-LSTM-based DL-NOMA receiver outperforms least square (LS) and minimum mean square error (MMSE) receivers. Furthermore, it has been discovered that the performance of the end-to-end system degrades with the growing amount of node mobility, or if CSI knowledge remains poor. Simulated curves are in close agreement with the analytical results.

Keywords — inter-symbol interference, MIMO, NOMA, orthogonal frequency division multiplexing (OFDM), S-LSTM, zero-mean circularly symmetric complex Gaussian (ZM-CSCG).

1. Inrtoduction

The market expects that 5G communications will be suitable for providing services with very low latency, excellent quality of service (QoS), and increased mobile broadband [1], [2].

Several technological advances, including 5G radio access networks (5G-RAN), the Internet of Things (IoT), ultra-reliable low-latency communications (URLLC), heterogeneous networks, including small cells and machine-to-machine (M2M) communications, as well as the understanding of the mechanisms of specific methodologies, are important building blocks of the 5G air interface [3], [4]. Vehicular communication (VC) solutions, such as vehicle-to-vehicle (V2V) and vehicle-to-infrastructure (V2I) schemes, are widely used in safety-, information-, mobility- and environment-related applications. Because of its unique characteristics, VC has evoked the curiosity of academics, businesses, and governments alike. V2V and V2I have been envisioned as one of the most promising schemes for improving traffic management and road safety, because they allow each vehicle to communicate with other users placed at important intersections, such as stop signs and traffic lights. A schematic representation of a V2V network is presented in Fig. 1 [1], [2].

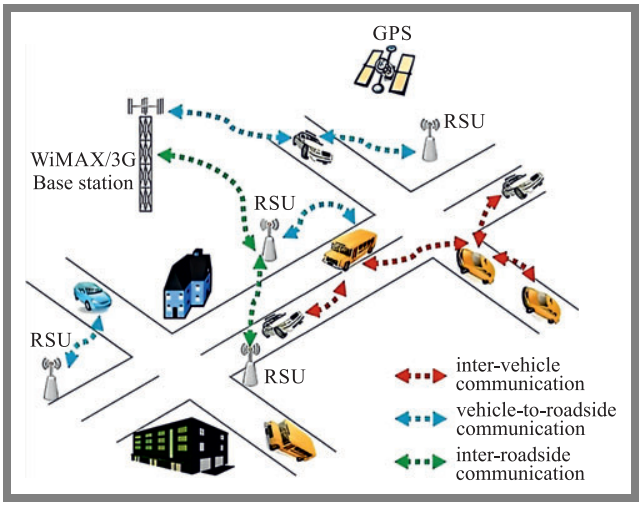

Fig. 1. Schematic representation of a V2V scheme.

In addition to being a new resource allocation scheme, 5G wireless networks rely also on a user-centric network concept that seeks to meet the application needs of all users participating in the connected world [5]–[7]. It is almost impossible to develop a unified technology that meets the broad variety of transmission-related needs, due to the sheer number of access schemes and use cases existing in today's interlinked, digital world. Therefore, 5G does not seek to alter the wireless 4G architecture, instead offering a unified platform that makes use of all current and envisioned technologies to serve users by providing them with access to a wide range of services. 5G aims to provide new air interfaces as well as a few new access modes by making relying on a spectrum that has recently been allocated. To be more specific, it will be built on top of contemporary wireless technologies, such as 5G URLLC, long-term evolution advanced (LTE-A), mmWave high-band 5G, lowest signal-to-interference-plus-noise ratio (SINR), and enhanced mobile broadband (eMBB).

It is crucial to outline the fundamental components of 5G in order to create a framework for the co-existence of other technologies. Secure communication in V2V and V2I NOMA networks demands minimal latency, excellent end-to-end reliability, and massive connectivity. Intelligent transportation systems (ITS) will be applied in entertainment applications, such as connected driving and smart transportation, thus increasing the requirement for spectral efficiency (SE) [8]–[11]. By enabling multiplexing in the code and the power domain, NOMA – which significantly improves energy and SE over orthogonal multiple access (OMA) – serves many users concurrently or simultaneously accessing frequency resources [12]. 5G, IoT and multimedia applications place strict demands on capacity and user access. The NOMA scheme [13], [14] offers an optimistic answer to these challenges. MIMO, cognitive cooperative relaying, full-duplex relaying, millimeter-wave, and other technologies have been employed in conjunction with NOMA to increase throughput and guarantee user fairness in a wide range of fading channel distributions [15], [16]. Figure 2 shows a MIMO-NOMA network example [10], [17].

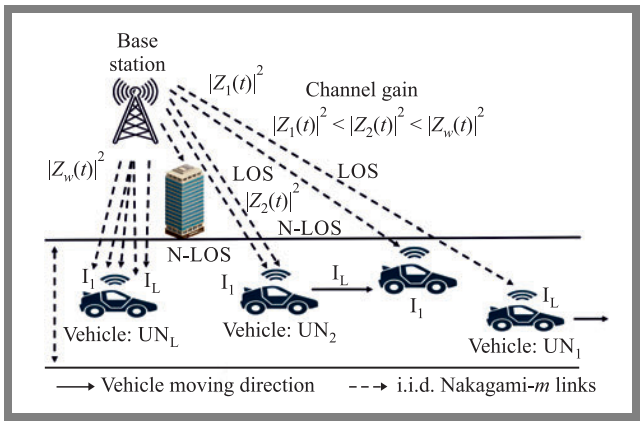

Fig. 2. V2V NOMA scenario over Nakagami-m fading channel conditions.

2. Related Work

In [18]–[20], the authors examine the millimeter-wave scheme over quasi static frequency flat links. Over the frequency flat α-η-κ-μ fading channels, paper [21] evaluates end-to-end SER performance of the relaying network in conjunction with a NOMA scheme for multiple users. In [22], cooperative NOMA's exact OP performance and the achievable data rate are examined by considering an analog relaying protocol over frequency-flat generalized Nakagami-m fading links, and in [23], the authors extend that work by considering imperfect CSI conditions and additive white Gaussian (AWGN) channel noise. It is very difficult to compare channel matrices in MIMO networks. In their work [24], [25], the authors propose the generalized singular value decomposition (GSVD) approach turning MIMO channels into several single-input single-output (SISO) channels [24], [25]. The authors look at how well MIMO-NOMA networks minimize delays when limits concerning transmission time and power are imposed. This study shows that MIMO-NOMA systems offer shorter delays than their OMA-based counterparts.

Since security is one of the paramount issues in wireless networks, the authors of [25] investigate how NOMA and OMA networks compare in terms of ensuring confidentiality of information. The results show that NOMA-MIMO offers a higher secrecy rate. Additionally, the effectiveness of NOMA has been assessed for partial CSI [26]. However, there are several restrictions affecting NOMA, including the need for a perfect CSI in the transmitter and a significant amount of processing complexity in the receiver.

Utilizing deep learning (DL) methods is a great way to overcome these difficulties. The traditional SIC technique has several drawbacks. With more users, it becomes more challenging to utilize the SIC approach to accurately interpret the data. Propagation inaccuracy also has an impact on the SIC approach. Signal categorization may be used by deep neural networks (DNN) to recover a discrete sequence from a degraded signal. The SIC approach can be improved with DL as well. The authors of [27] study a beamforming-based downlink NOMA network that uses dynamic user pairing to maximize the lowest data rate of all DL users. The authors resolve the issue with non-convex optimization with mixed-integer variables, by converting a discrete domain to the analog domain using an iterative scheme depending on the internal approximation to obtain a local optimum. The suggested technique outperforms standard beam generation, NOMA with random pairing, and heuristic search schemes.

DL is a popular channel estimation approach used in 5G networks. Traditionally, channel estimation and signal detection processes are separated. Before signal detection, a pilot broadcast estimates CSI. The receiver may reconstruct the transmitted signals using the calculated CSI. End-to-end OFDM channel analysis is discussed in detail in [28], describing a DL-based technique for joint channel estimation and detection in OFDM systems. Training a DL model involves matching the received signals with the data and pilots provided. After training, the model can decode online-transmitted data without channel estimations. Furthermore, the authors analyze a DL-based single-input multiple-output (SIMO) channel estimate. By using piecewise linearity, the DL channel detector might be able to estimate a large group of functions, since a DNN with a rectified linear unit (ReLU) activation function is conceptually similar to a piecewise linear function. An alternative method for estimating the channel using the DL scheme is presented by the authors in [29]. The authors provide an alternate method for DL channel estimation. MMSE is a model-specific estimator for conditionally normal channels. Using MMSE, CNN estimators are defined.

Due to the high processing complexity and substantial variations in wireless channel conditions, current NOMA systems make it difficult to evaluate channel characteristics and establish the appropriate resource allocation strategy. In [30], the authors present a DL-aided NOMA system, where a single BS serves random NOMA users. DL learns time-selective fading NOMA systems with poor CSI. DL-LSTM networks

in NOMA systems provide automatic channel property identification. NOMA employs DL for automatic encoding, decoding, and channel identification in AWGN noise. The suggested method provides more accurate simulations. Faster than Nyquist (FTN)-NOMA is proposed in [31] to improve SE, reduce latency, and increase connectivity. The authors define sliding-window detection for DL-based FTN NOMA. This scheme's detector exceeds MMSE-decision feedback equalization (FDE).

In [32], the authors suggest DL-SIC for downlink (D/L) MIMO-NOMA. This method minimizes MMSE in MIMO-precoding NOMAs and SIC decoding. The transmitter precodes signals for multiple D/L users using superposition coding, and the receiver extracts them using DNN-built SIC decoders. In each of the SIC phases, one DNN is used to decode the signal for the current user, while another is used to reconstruct the signal for the prior user (apart from the first user). Since the user was not previously decoded, just one DNN is required to decode the signal. In [33], the authors establish a DL approach for recognizing D/L signals using the MIMO-NOMA scheme. DNN is the sole SIC receiver used to decode D/L signals broadcast in a single time slot. All aerials provide DNN with data. Most DNNs have a fully linked output layer that uses the Softmax function. Conversely, MIMO-NOMA signals, although emanating from several different transmitters, need a single decoding slot only. Therefore, the proposed output layer is constructed for data classification purposes. Each cluster has as many neurons, as there are aerials for sending signals, and each neuron in a cluster may only be capable of encoding a single state. Different power allocations and complex modulation forms degrade energy efficiency of the proposed system.

Using DL schemes such as CNNs, the authors of [34] reconstruct uplink users' MIMO channel signals. Data from several users may potentially be decoded instantly using the suggested technique which does not rely on any of the typical processes found in communication signal processing. Each step of the SIC decoding procedure in [35] employs a DNN with fully linked layers to decode input from a single user. DNN is composed of four layers: an input layer, an output layer, two hidden layers, and an intermediate hidden layer. The decoded bits that are shown to the user are generated by the DNN's output layer which is responsible for that function. After the first stage of SIC, the input layer receives the combined signal in addition to the signals that have already been decoded by the users. Signals must be transformed into bit sequences before digital neural networks (NNs) (also known as DNNs) may be trained to interpret them. The method provided in [35] to enhance DL-based SIC systems for higher order modulation will be shown in Section 3.

2.1. Contribution of the Paper

DL is a popular approach relied upon for boosting error performance of MIMO-NOMA end-to-end systems. DL-based SIC uses a NN to estimate, identify, decode, and reject channels. DL-based SIC outperforms MIMO NOMA in Nakagami-m fading channels. We apply the DL-based SIC from [35] to an uplink MIMO-NOMA system with BPSK modulation in a time selective Nakagami-m fading channel conditions, and then:

– study the DL-based MIMO NOMA VC system over Nakagami-m fading channel users and compare it with the conventional SIC-based NOMA system,
– study the DL schemes for 5G and beyond 5G communications, with a focus on the VC scenario and the imperfect CSI and conduct a comprehensive literature research on DL,
– for different values of the shape parameter, training data rates, and packet sizes, the traditional NOMA receiver's performance is compared with that of the S-LSTM-based NOMA receiver,
– to decode user signals and ensure performance with current conventional systems, it is necessary to create a DL-SIC MIMO-NOMA model for higher-order complex modulation schemes using the newly suggested architecture.

The paper is organized as follows. Assuming that CSI is imperfect and that a SIC error exists, we examine the signal and channel models in Section 3. The node mobility scenario is considered in this section, and the effects of channel estimation inaccuracy are investigated. We analyze the DL-based NOMA receiver in Section 4 and present the S-LSTM approach for enhancing both OP performance and end-to-end SER. Optimal power allocation (OPA) is determined because of a derivation for the ideal power allocation factor. Additionally, training for the S-LSTM model is provided. We discuss the simulation's outcomes in Section 5, and we conclude the study in Section 6.

3. System and Channel Model

3.1. Channel Model

As a result of multipath propagation and node mobility, fading links transform from being frequency-flat to time-selective. ISI is caused by time-varying channels and 5G-OFDM uses a cyclic prefix (CP) to reduce it [36]–[42]. In this work, the MIMO technique is employed by the base station (BS) in order to connect with W vehicular nodes (VNs) in NOMA-based V2V communication networks [10]. As the VN moves away from the BS, the fading channel profile changes from the near Rician-fading channel to a Rayleigh channel. With the help of singular value decomposition (SVD) techniques, the channels are converted to parallel fading links. To take advantage of the diversity at the VNs, the receiver uses maximum ratio combining (MRC), selection combining (SC), or SVD schemes. However, because the diversity of connections is non-identical under high fading conditions, the predicted diversity increases when the independent but non-identically distributed (i.n.i.d.) assumption is not realized [10], [30]. The i.i.d. assumption adds complexity to the study, but the conclusions are more realistic and relevant in real-time communication and V2V network system design [38],

[42]. Here, we analyze the performance of an S-LSTM-based V2V NOMA networks over i.i.d. fading connections while accounting for inaccurate CSI, and we compare findings with the existing literature. This section also examines wireless D/L V2I communications and considers the time selective Nakagami-m model.

Mobile users communicating with a roadside BS move away from that BS at a comparable v speed. Each VN has T receive (Rx) antennas, whereas the BS has K transmit (Tx) antennas. Doppler spread is experienced due to the relative motion between the VNs and the BS. i.i.d. Nakagami-m fading links can be modeled by using the classical Jakes model and the first order autoregressive model. The fading channel coefficients between the BS and w vehicle at t time interval are expressed as [10], [17]:

$$z_w(w) = \rho_w^{t-1} z_w(1) + \sqrt{1-\rho_w^2} \sum_{l=1}^{t-1} \rho_w(t-l-1) e_w(l), \quad (1)$$

where $\rho_w = J_0 \frac{2 \cdot \pi \cdot f_c \cdot \nu}{R_s c}$ is the correlation factor for the gain of the temporally neighboring channel, the carrier frequency is denoted by f_c, c is the light speed [4]–[8], [33], and transmission symbol rate is represented by R_s. The zeroth-order Bessel function of the first kind is defined as $J_0(:)$. The time selective fading component is represented as $e_w(l)$ which is modeled as the ZM-CSCG with variance σ_{ew}^2.

According to the working theory, destination tracking loops are unable to keep up with time-varying channel variances and can only estimate them during the first signaling period of each transmitted block, because node mobility causes the fading channel coefficients to change for each time instant and transform a quasi-static Nakagami-m fading channel into a time selective fading channel. This is because the quantity of information that may be communicated is limited by the time selected Nakagami-m fading connections, i.e. $z_w(1)$ as $\hat{z}_w(1)$. Furthermore, ISI and channel estimation error $\hat{z}_w(1)$ can be expressed as:

$$\hat{z}_w(1) = z_w(1) + \hat{z}_{\epsilon w}(1),$$

where $\hat{z}_{\epsilon w}(1)$ is the fading channel error coefficient distributed as ZM-CSCG with variance σ_ϵ^2 modeled as, $\mathbb{CN}(0, \sigma_e^2)$. The small-scale fading channel is affected by the path loss. The estimated value of the fading channel coefficient $\hat{z}_w(1)$ is affected by the path loss exponent ϵ, as a function of distance d_w between BS and mobile user w . At $t = 1$, the gain of the fading link is given as, $\hat{z}_w(1)|^2$ [5], [6], [17], [33]–[35]. The fading channel link gain is inversely proportional to the distance from the BS to mobile user w. With the increasing distance between the BS and the user, channel gain decreases. At $t = 1$, the channel gain is:

$$|\hat{z}_1(1)|^2 \leqslant |\hat{z}_2(1)|^2 \leqslant \ldots \leqslant |\hat{z}_W(1)|^2.$$

The BS uses superposition coding and power domain NOMA to correlate the signals for various vehicles in the power domain. When considering the channel order at time t, the power coefficients assigned to vehicles are expressed in the following order $\beta_1(t) \geqslant \beta_2(t) \geqslant \ldots \geqslant \beta_W(t)$ [3]–[7], [33].

3.2. System Model

The use of DL to increase the performance of MIMO-NOMA systems has recently gained in popularity. SIC-related research based on DL uses a neural network (NN) to conduct channel estimation, detection, decoding, and discarding of the decoded signal. A DL-based SIC receiver performs better than MIMO-NOMA under Nakagami-m fading channel conditions. Hence, under time-selected Nakagami-m fading channel conditions, we apply a modified version of the DL-based SIC, as suggested in [35], to the uplink MIMO-NOMA system that uses BPSK modulation. After analyzing DL-based SIC in [35], the system model is formalized and DNN is applied in the SIC receiver.

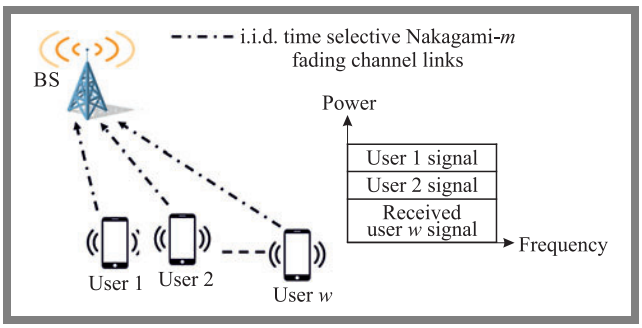

Fig. 3. Schematic representation of uplink in a MIMO NOMA (single cell) network.

Figure 3 illustrates the single cell uplink MIMO-NOMA scenario over time selective Nakagami-m fading channel conditions. The receiver has T antennas, and W represents the total number of users. The schematic diagram demonstrates that users are broadcasting their signals to the BS utilizing the same frequency resources, but at varying degrees of transmission power. According to the findings from [35]–[43], the users must transmit many frames which include both pilot and data symbols. When the frames are sent within a coherent period, the channel impulse response is assumed to be constant across the span of a single frame. Each frame has N data symbols and J pilot symbols. Symbols with the letter L in front of them are considered pilot symbols, whereas those with the D letter denote data symbols. Inspired by the analysis in [35], all users' data signals are expressed as [35], [43]–[45]:

$$\mathbf{R} = \mathbf{ZP}\mathbf{S}^D + \mathbf{\Psi}^D, \quad (2)$$

where S^D represents the data matrix as:

$$S^D = [S_1^D, S_1^D, \ldots, S_W^D]^{\mathrm{T}} \in \mathbb{C}^{W \times N},$$

where T is the transpose operator, W represents the total number of users, while the total number of receive antennas is T. S_w^D denotes the data vector of w-th user complex modulated data symbol and can be given as [35], [44], $S_w^D = [S_{w,1}^D, S_{w,2}^D, \ldots, S_{w,N}^D]^{\mathrm{T}} \in \mathbb{C}^{1 \times N}$ and $E(|S_{w,N}^D|^2) = 1$. The fading channel matrix $\mathbf{Z}$ is represented as [30]–[35]:

$$\mathbf{Z} = [z_1, z_2, \ldots, z_W] \in \mathbb{C}^{T \times W},$$

where $z_w = [z_{w,1}, z_{w,2}, \ldots, z_{w,T}] \in \mathbb{C}^{T \times 1}$ is the channel vector between w users. Considering the time selective Nakagami-m fading channel conditions, let the diag-

onal matrix P be represented as [35], [43], [44], [46] $P = \text{diag}(\lambda_1, \lambda_2, \ldots, \lambda_w)$. P represents the total available transmit power and is equal to $\sum_{w=1}^{W} \lambda_w \leqslant P$. Ψ^D is the AWGN noise at the BS modeled as $\Psi^D \sim \mathbb{CN}(0, N_0 I) \in \mathbb{C}^{T\times N}$. The same approach can be used to represent all users' pilot signals at any frame [34], [35], [43], [44], [46], [47]:

$$\mathbf{R}^L = \mathbf{ZPS}^L + \mathbf{\Psi}^L \tag{3}$$

with energy of the symbol equaling:

$$E(|S_{w,n}^L|^2) = 1.$$

S^L stands for the pilot matrix and can be expressed as [44]:

$$S^L = [S_1^L, S_2^L, \ldots, S_W^L]^{\mathrm{T}} \in \mathbb{C}^{W\times J}.$$

Channel noise $\Psi^L \in \mathbb{C}^{T\times J}$ is assumed to be AWGN noise for pilot symbol transmissions at the BS. In articles [35], [43], [44] the authors have considered the equal power allocation scheme. Paper [46] analyzes mMTC with the assumption that all mobile users have access to the same bandwidth. There are several drawbacks to the equitable distribution of power. The user should be allocated less power if they are close to the BS, since the channel gain between them is higher than it would be otherwise. Due to its poor channel gain, the distant user needs a larger share of the available power. Using the dynamic power distribution technique in [35], [43], [44], [46], [47], the authors provide more power to the user with the lowest gain, while giving less power to the user with the highest gain. Availability of power at the BS is limited - let it be represented by P. The total available power is distributed among W users. The power allocation factor λ_w is expressed as [30]–[34]:

$$\lambda_w = \frac{P}{W} \;\; \forall\, w \in \{1, 2, 3, \ldots, W\}.$$

Let user 1 be nearest the BS user w is the farthest user. Channel gain decreases with distance, as $||z_1|| \geqslant ||z_1|| \geqslant \ldots \geqslant ||z_W||$. Detecting the received signals involves recovering the signal at the receiver. A standard MIMO-NOMA receiver must perform channel estimation, signal detection, and demodulation before extracting the signal. The operation of a conventional SIC receiver is shown in Fig. 4. The strength of the signals provided by users will be used to discern their meanings. To do this, we start by decoding the user who is experiencing optimal channel circumstances, and then we deduct their signal from the composite signal. Then, the user with the second-highest signal strength will have their code decrypted. The process will be repeated until the individual user whose signal strength is the weakest can be deciphered.

Operation of SIC is determined by the user count. S_w^L pilot symbols allow the channel to be estimated during the pilot broadcast. Using zero forcing (ZF)-SIC and MMSE SIC, MIMO-NOMA can successfully cancel interference. The data vector (estimated value) for mobile user w can be obtained by employing the ZF-SIC receiver as [21], [33]–[35], [44], [46]:

$$\hat{S}_w^D = Z_w \mathbf{R}^{\mathbf{D}}, \tag{4}$$

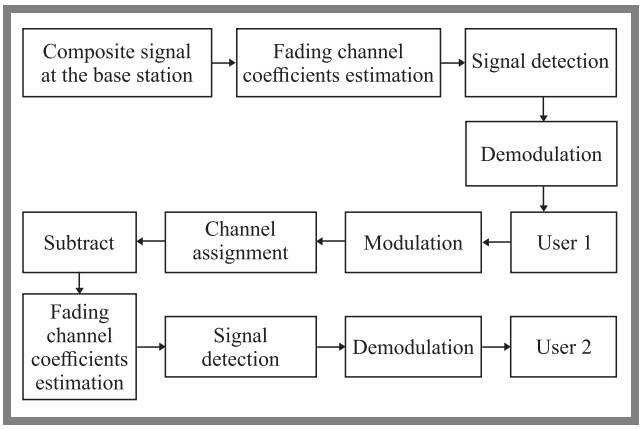

Fig. 4. Schematic representation of a SIC-based receiver.

where $\hat{z}_w$ is the channel estimation vector of user w, as:

$$\hat{z}_w = [\hat{z}_1, \hat{z}_2, \ldots, \hat{z}_T]^{\mathrm{T}} \in \mathbb{C}^{T\times 1} \text{ and}$$
$$Z_w = \hat{z}_w^H (\hat{z}_w \hat{z}_w^H + I)^{-1}.$$

Next, the $(w+1)$-th user's signal is decoded after the decoded signal is subtracted from the received signal. Similarly, the detection for user w using MMSE-SIC may be written as [32], [35], [37], [43], [44], [46]–[48]:

$$\hat{S}_w^D = W_w \mathbf{R}^{\mathbf{D}}. \tag{5}$$

where $W_w = \hat{z}_w^H (\hat{z}_w \hat{z}_w^H + \rho^{-1} I)^{-1}$ and ρ is the received SNR given by [30], [33]–[35], [43], [44]:

$$\rho = \frac{P_r}{N_0}. \tag{6}$$

Also, the SINR of user w is given as [30], [33]–[35], [43], [44]:

$$\text{SINR}_w = \frac{\lambda_w \rho |z_w|^2}{\sum_{j=1}^{w-1} \lambda_j \rho |z_j|^2 + 1} (w \neq 1). \tag{7}$$

Furthermore, the SINR calculation for user 1 is [30], [33]–[35], [43]–[46]:

$$\text{SINR}_1 = \lambda_1 \rho |z_1|^2. \tag{8}$$

To communicate with the SIC receiver, the DNN protocol has been established. According to the results of the preceding research, a standard SIC receiver starts by making an estimate of the CSI based on the transmitted symbols that match the pilot symbols. The estimated CSI may then be used for reconstruction of the received signal. The DNN, in contrast to the DL-based SIC technique, is trained during the pilot transmission and then utilized to recover the transmitted bits without explicitly calculating the channel state or discarding the decoded signal. This is possible because the DL-based SIC approach makes use of DL.

To decode the data from a single user, a DNN with layers that are completely linked is used at each stage of SIC. In addition to input and output layers, the DNN design includes two hidden layers. Except for the first SIC step, the DNN output layer decodes bits for each user, whereas the input layer receives the composite signal and previously decoded signals. DNNs are trained to convert the input data matrix into bit sequences for the broadcast. The user with the best

channel condition would have their data deciphered first, as in the traditional SIC system. Then, in SIC, the second-strongest user is decoded. In this manner, the procedure is repeated to decode the user at the lowest level. Modulation order C is used to determine which nodes of each DNN will be used as outputs. BPSK requires two nodes, whereas BPSK needs four. Figure 5 shows a two-user DL-based SIC architecture. After each DNN SIC, the next modulation block modifies the decoded user bits. During SIC, the user's modulated symbols are delivered to DNN.

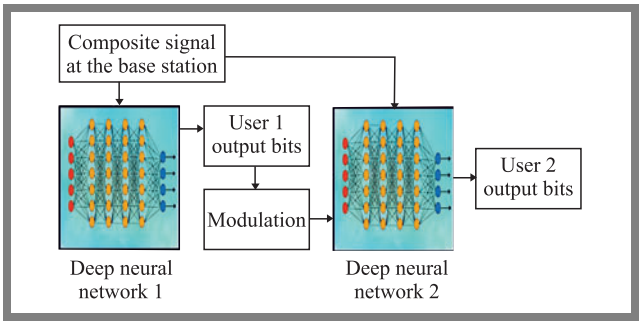

Fig. 5. Schematic representation of a DL-based SIC receiver.

DNN is composed of Q fully linked layers, and the Softmax function is used on the output layer of each DNN. Firstly, we consider the input vector $\mathbf{s} = \{s_1, s_2, \ldots, s_c\} \in \mathbb{R}^{C\times 1}$ and we can find a way to express the output vector $\Phi = \{\Phi_1, \Phi_2, \ldots, \Phi_C\}$ using real number values in the range of 0 to 1 that add up to 1 [48]. The Adam algorithm optimizes performance by decreasing the categorical cross-entropy loss function between output and training objectives. The loss function is given as [32], [35], [43]–[48],

$$\text{loss} = \sum_{j=1}^{J}\sum_{c=1}^{C} B_{jc} \log\left(\frac{\Phi_{jc}}{2}\right), \tag{9}$$

where B_{jc} is a binary ground truth indicator such that $B_{jc} = 1$ only holds if and only if the j-th sample belongs to the c-th class. The Softmax's output probability that the j-th input corresponds to the c-th class is represented by the Φ_{jc} symbol. Consider $f_w(.)$ to be the w-th DNN's processing component, with function $f_w(.)$ defined as $f_w(.) : \mathbb{R}^{(T+w-1)} \rightarrow \{0,1\}^{\log_2(c\times 2)}$, which maps the combined signal and the previously decoded signal of the $(w-1)$-th users to the broadcast bit of user w [49]–[53]. This is possible because all users' complex signals can be split into real and imaginary parts. To estimate the function of the w-th DNN, the weight and bias matrix are changed after pilot symbol training. Specifically, ELU and ReLU are used as activation functions for the first and second hidden layers.

4. DL Based NOMA Receiver

4.1. S-LSTM Basics

LSTM cells are presented in Fig. 6 [31]–[33]. Recurrent neural networks (RNNs) are known as LSTM networks, and they can learn the long-term associations that exist between sequence time steps. An LSTM network is made up of several different layers, two of which are the sequence input layer and the LSTM layer. A sequence input layer is a component of the network that is responsible for the transmission of data to the network in the form of sequences or time series. An LSTM layer will learn the long-term connections that exist between the many time steps that make up the sequence data. The LSTM architecture is shown in Fig. 7 [32], [33]. The sequence input layer is followed by the LSTM layer. Three layers are used to forecast class labels: a fully connected layer, a Softmax layer, and a classification output layer. Figure 8 [32], [33] shows a basic regression LSTM network. The first two network layers are sequence input and LSTM. The network's last layers are completely linked and regressed.

Figure 9 shows the video classification network architecture. The image sequences could be networked with the help of a sequence input layer. To independently apply convolutional processes to individual video frames, each frame needs to include a sequence folding layer, followed by convolutional layers, and finally a sequence unfolding layer. To use LSTM layers to learn from vector sequences, we must first deploy a flattened layer – Fig. 9 [32]. In its most basic form, an LSTM model comprises a single hidden LSTM layer followed by a feed-forward output layer. S-LSTM is a variant of this paradigm that includes several hidden LSTM layers, each with numerous memory cells. As more and more LSTM hidden layers are stacked, the model becomes more complex, and the technique becomes more acceptable as DL. The hierarchy provided by the DNNs' several layers is frequently credited with its effectiveness. Each layer solves a smaller subproblem before passing the solution to the next layer. The DNN may be thought of as a processing pipeline, with each layer performing a specific task and passing the data on to the next layer to be processed.

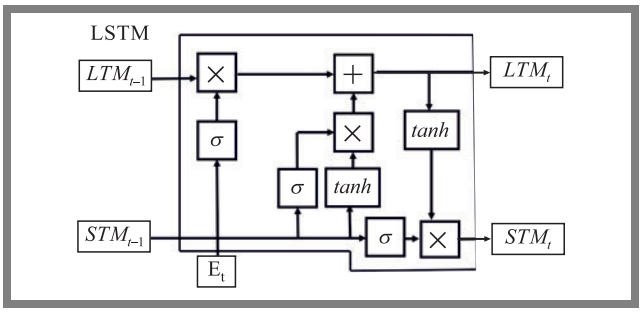

Fig. 6. Schematic representation of an LSTM cell.

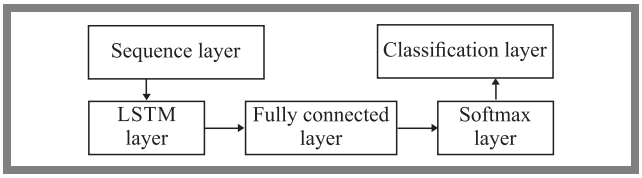

Fig. 7. Schematic representation of a simple LSTM network for classification.

Adding extra hidden layers to an NN multilayer perceptron makes it more complex. High degrees of abstraction can be achieved by combining the learnt representation from pre-

vious layers with the additional hidden layers. Lines, forms, and objects are just a few examples here. A single, suitably deep hidden layer. Most functions may be approximated using multilayer perceptrons. An alternative approach that uses fewer neurons and trains more quickly involves deepening the network. After all, depth optimization is a form of representational optimization.

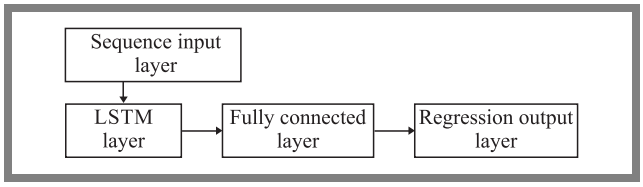

Fig. 8. Schematic representation of an LSTM network for regression.

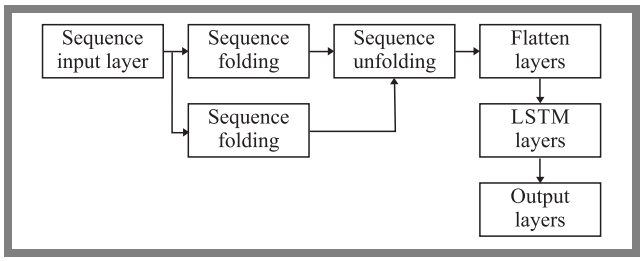

Fig. 9. Schematic representation of a video classification network.

In [25], the authors proposed S-LSTM or deep LSTMs for their speech recognition application. The authors achieved this by solving a difficult standard problem. RNNs are deep in time, because they use hidden states. This paper examines the question of whether RNNs may also take advantage of the benefits of depth in space, i.e. the practice of placing numerous, recurrent hidden layers one atop the other, the way that feedforward layers are built in conventional deep networks. Layered LSTMs have recently solved difficult sequence prediction tasks. S-LSTM architecture is a name given to an LSTM model that is made up of multiple, different layers of LSTMs. A higher-level LSTM transmits values to a lower-level LSTM. Each input time step should have a separate output time step (Fig. 10), instead just of one such step. It is necessary to generate one output time step for each input time step, and to generate one output for each input [29].

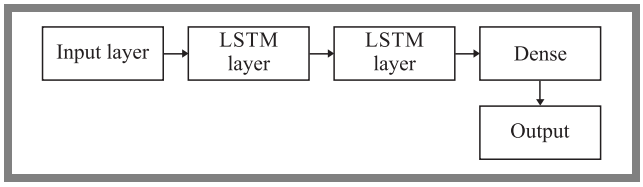

Fig. 10. LSTM architecture.

4.2. Model Training

OFDM data packets consist of 92 carriers, and each packet consists of four OFDM symbols. Three pilots are assigned to detect fading channel coefficients. The number of bits per carrier is 4, because channel detection is a very complex task and more bits are assigned per subcarrier. After the carriers have been assigned, the next step is to create a feature vector (FV) and, despite the fact that data symbols are of a complicated nature in the training stage, this step must be completed before moving on. The symbols include both real and imaginary components in their construction. The number of subcarriers influences the size of the FV in a significant way. The FV dimension may be expressed as $92\times4\times2 = 736$. The S-LSTM NOMA channel estimator acquires the ability to comprehend the signal connected to the k-th subcarrier after having the key labels included in the training process. A label is a numerical representation of a signal sent by two users together. There will be 30 combinations/labels, since BPSK symbols are being transmitted by both users. DNNs are created with Python and Matlab by attaching DL layers to the DL Toolbox and GPU accelerator. Tensor flow and the Sigmoid activation function are employed in the receiver analysis. A fully linked layer comes after the S-LSTM layer. This layer has an output size of 30 bits and contains 280 hidden units. The classification layer is responsible for generating putative labels that will be used to map the signals that are being concurrently sent by both users, and the Softmax layer is the one that will apply a Softmax function to the input.

5. Simulation Results

In this section, performance comparisons have been presented between S-LSTM and other conventional NOMA receivers, in terms of node mobility, SIC error, and imperfect CSI. Further, the S-LSTM NOMA receiver is trained using simulation data and the end-to-end SER and OP are examined. Performance of the system is investigated for each subcarrier, over the various SNR regimes. The effect of ISI and Doppler spread is thought to be reduced in both online training and offline training by assuming that the fading links are time-selective and there is imperfect CSI. All i.i.d. fading links receive a distinct random face shift from each OFDM packet, enabling the analysis of time-selective fading channel conditions. This proposed scheme is trained using 550,000 OFDM samples over 280 epochs, while considering all real-time propagation scenarios, i.e. those involving SIC error and imperfect CSI. The accuracy of S-LSTM-based receivers is evaluated using optimal or maximum probability receivers. In simulations, the carrier frequency is 25 GHz, CP duration is 20 and 25 s, the number of subcarriers is 92, and the number of multiple paths is 60, 70, 80, and 90. BPSK constellations have been used, and the maximum delay spread is set to 25 μs. Table 1 shows the simulation parameters.

5.1. OP Performance in Time-selective Fading Channels with VNs and Imperfect CSI

OP performance and average SER performance of the different modulation schemes for NOMA-based 5G V2V networks have been compared to validate the analytical findings given in the preceding sections. Consider a D/L V2V scenario in which all VNs are moving away from the BS at 130 km/h. The BS establishes connections with VN_1, VN_2, VN_3 and

VN_4 using the carrier frequency of $f_c = 25$ GHz and the transmit symbol rate of $R_s = 20$ Mbps. Assume that VN_1 is the farthest user, and that it has a weak fading channel gain. The channel gain also decreases significantly when the VN_1 moves away from the BS. For VN_2, the user closest to the BS, channel status fluctuates or is inversely proportional to distance and node mobility in the simulations. Channel coefficients change very fast, and gain is highly reduced as node mobility rises. For 25 GHz and 30 GHz frequency bands, the path loss exponent values are 1.64 and 3.10, respectively. The power allocation factors in the simulations for VN_1, VN_2, VN_3, and VN_4 are 0.60, 0.25, and 0.10, 0.05, respectively. The dynamic power allocation approach is employed. The target data transmission rate is fixed at 2 bps/Hz, yielding the threshold SNRs of 2, 4, 6, and 8 for VN_1, VN_2, VN_3, and VN_4, respectively. An autoregressive process with a variation of 0.01% at a certain point in time may be used to simulate a time-selective fading channel.

Tab. 1. Simulation parameters.

Simulation settings	Type or value
Total number of vehicular users	10
Number of Tx/Tr	20/10
DL optimization scheme	Stochastic gradient descent
Training rate	0.004
Number of complex modulated symbols	5000
Number of hidden layers	280
Hidden layer activation function	Parametrized ReLU
Number of training epochs	280
OPA factor	0.75, 0.25
Complex modulation scheme	BPSK
Fading channel used in simulation	Time selective i.i.d. Nakagami-m fading links

Algorithm 1. MIMO-NOMA DL-based training algorithm

1. Initialization of the DL model
2. Parameter initialization
3. Data normalization
4. Generation of training data symbols and formatting of the data symbols. In simulations, the total number of time slots is Ts and the data vector is: $S^L = [S_1^L, S_2^L, \ldots, S_W^L]^{\mathrm{T}} \in \mathbb{C}^{W \times J}$. The l-th slot time slot data is $S^{[l-\mathrm{th}]}$.
5. Set the hidden layer and output layer's important settings, including epochs, data training rate, dropout, and output functions
6. Assigning bias and weight to DNN layers
7. Calculation of the output data vector
8. Calculation of the loss function as: $\mathrm{Loss} = -\sum_{j=1}^{J} - \sum_{c=1}^{C} -B_{jc} \log(\frac{\Phi_{jc}}{2})$
9. Use the stochastic gradient descent technique to compute the correction parameter and to update the simulation settings to seek OPA factors that provide the minimum SER and OP
10. If the loss function is not satisfactory, then recalculate the loss function
11. Using the test data, evaluate the trained DNN and generate OP vs. SNR and OP vs. SNR plots

Figure 11b shows the user's OP performance for S-LSTM MIMO-NOMA and MIMO-OMA for *m*=3. When compared to $m = 2$, the performance is better, since the diversity of benefit for $m = 3$ is better (severity of fading decreases with an increase in the value of the fading severity parameter). It can be readily seen that MIMO-NOMA outperforms MIMO-OMA when $m = 3$, by a difference of 4 dB. However, the performance decline brought on by i.i.d. consideration is more pronounced when $m = 3$, as opposed to $m = 2$. The influence of i.i.d. consideration is shown to decrease under non-line of sight conditions. Because in non-line of sight communication, the channel is no longer Rayleigh faded,

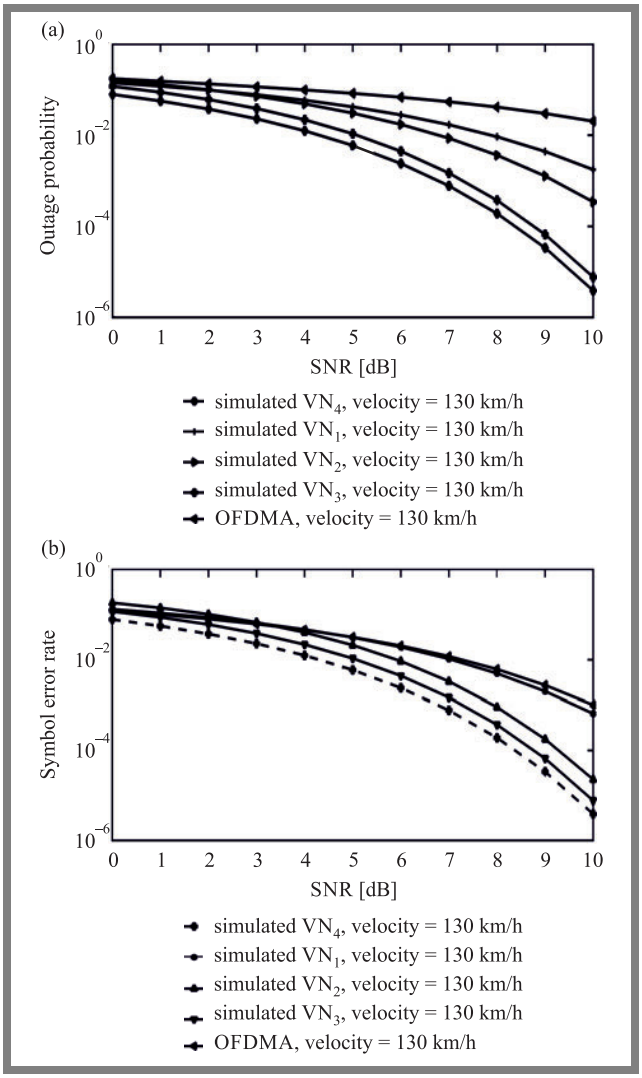

Fig. 11. OP vs. SNR for MIMO NOMA considering node mobility and imperfect CSI: a) $m = 2$ and b) $m = 3$.

and in this simulation, we have considered the time selective Nakagami-m, with more generalized fading. OP performance for $m = 4$ and 8 for the maximal ratio combining (MRC) NOMA and OMA is shown in Fig. 12a–b. Because $m = 4$ has more severe fading, $m = 8$ has better OP performance for 1×4 and 1×8 than $m = 4$. It can be readily seen that the simulation results differ from the analytical results if the likelihood of error is less than 10^{-4}. This is because the simulation's sample size was practically limited owing to computer-related restrictions.

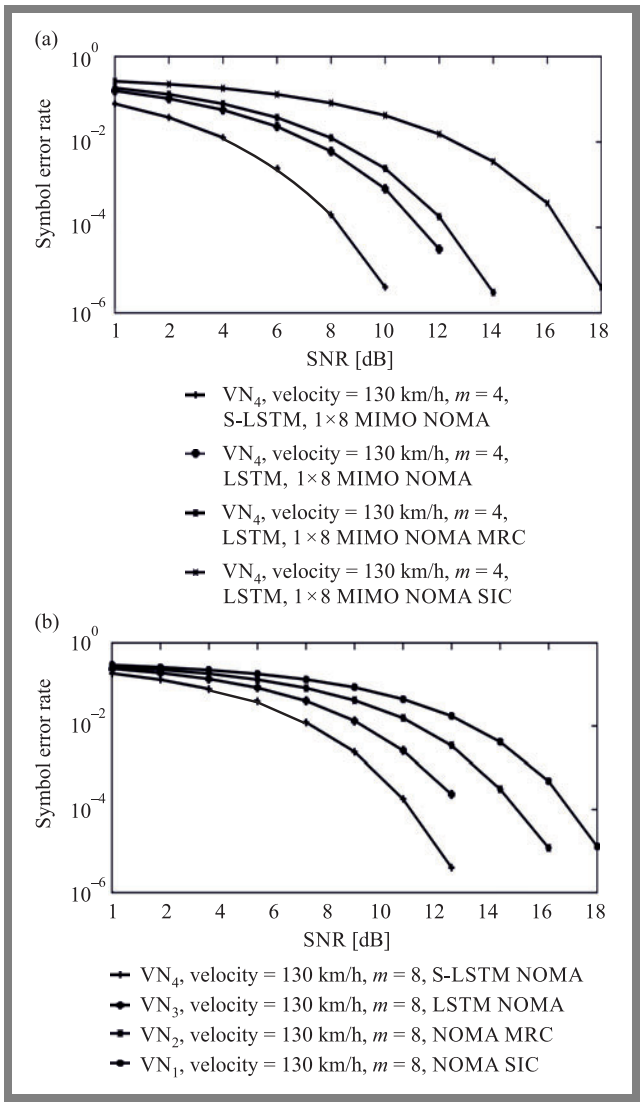

Fig. 12. OP vs. SNR for 1×8 and 1×4 MIMO NOMA for: a) $m = 4$ and b) $m = 8$, considering node mobility and imperfect CSI and error variance equal to $\sigma_\epsilon^2 = 0.02$.

Figure 13 shows a MIMO-NOMA with 4×2 and 8×4 antenna configurations, with imperfect CSI. The simulation results show how imperfect CSI error impacts the functionality of UN_2 and UN_3. UN_2 is affected by interference from UN_1, whereas UN_3 is affected by interference from both UN_1 and UN_2. As a result of an increase in SIC error, it is seen that UN_3 exhibits a greater rate of performance deterioration than UN_2. For both vehicles, 8×4 MIMO performs better than MIMO because of its higher diversity gain. Simulations of the net throughput and sum-rate between two VNs are performed for SISO-NOMA, SIMO-NOMA, and MIMO-NOMA. The power coefficients for UN_1 and UN_2 are $\beta_1 = 0.70$ and $\beta_2 = 0.30$, respectively, while the i.i.d. channel has a decaying factor of 0.40. It is assumed that the receiver has access to the ideal CSI. MMSE channel estimation also shows the sum rate performance. Periodically, the BS transmits pilot signals for the purpose of channel estimation. Even if the velocity is higher in the case of S-LSTM when compared to the S-LSTM scheme, SER performance is better compared to the LSTM NOMA scheme. This is something that can be clearly recognized.

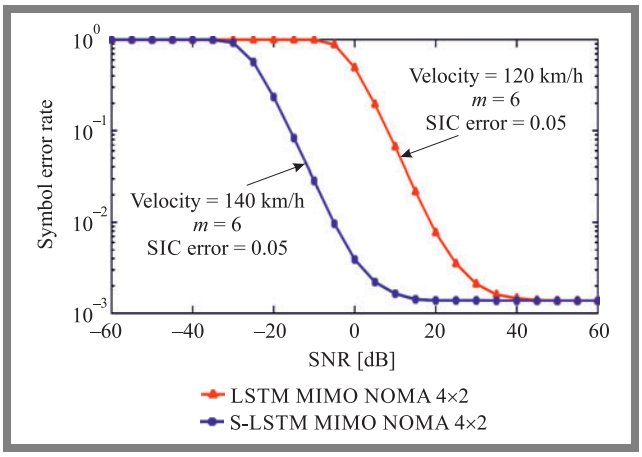

Fig. 13. Performance comparison between the 8×4 and 4×2 MIMO NOMA system over time selective Nakagami-m fading channel considering SIC error.

5.2. Effect of the Number of Pilot Symbols and Clipping Noise

As shown in Fig. 14, both MMSE and LS approaches may produce accurate estimates and detection rates when 120 pilots are used. Standard MMSE, LS, and SIC-based receivers are outperformed by the S-LSTM based NOMA detector. MMSE and SIC-based receivers' detection accuracy decreased by 15 dB SNR after limiting the number of pilots to 35, for both VN_1 and VN_2. Additional pilots make it abundantly evident that when the velocity between communication nodes rises, the fading links transform from being frequency-flat to time-selective, resulting in a decreased SER. However, the DL NOMA receiver can equal the performance of the 120-pilot example. This demonstrates that the S-LSTM-based receiver is more dependable for many pilots and can attain a higher level of performance with a lower number of pilots.

In Fig. 15, a comparison of performance is provided for various values of CP. Considering the scenario in which $length_{CP}$ is greater than $length_{impulse\ response}$, DL NOMA works considerably better as opposed to the scenario the $length_{CP}$ is less than $length_{impulse\ response}$. Because the channel is changing at every instant, it has been demonstrated in the literature [12]–[16] that neither MMSE nor LS schemes can properly detect the fading channel coefficients. Due to the ISI effects caused by temporal selectivity, the ideal ML-based NOMA receiver can no longer provide the optimal response, even in the event of perfect CSI. In a real-time communication scenario,

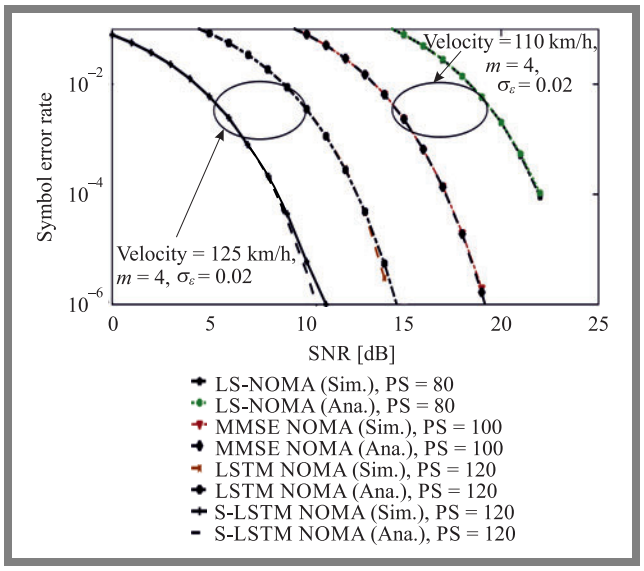

Fig. 14. Performance comparison between S-LSTM and conventional NOMA receivers for various pilot numbers, considering node mobility and error variance equal to $\sigma_{\epsilon}^2 = 0.02$.

frequency-selective links are needed to check the robustness of the S-LSTM NOMA receiver.

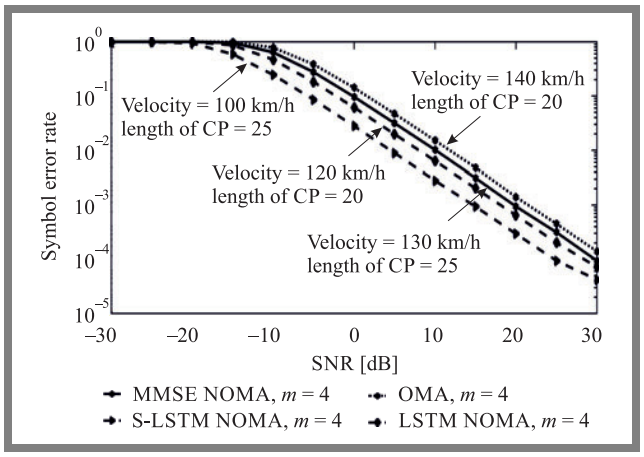

Fig. 15. Performance comparison between S-LSTM and conventional NOMA receivers for various CP length values, considering node mobility and channel error variance equal to 0.02.

When the influence of node mobility is disregarded, the S-LSTM NOMA receiver's end-to-end error performance under frequency flat fading channel circumstances is in near agreement with the ideal ML-based NOMA receiver. Additionally, the end-to-end error performance of the Nakagami-m connections considerably improved as the shape parameter or amount of fading was increased. Additionally, the S-LSTM NOMA detector for VN_2 (far user) in Fig. 16 is robust in terms of signal intensity and has an impact on conventional error estimation. Performance of the DL NOMA detector is equivalent to the optimal fading channel circumstances and is more resistant to random channel fluctuations.

The simulated results have demonstrated that a reduction in node velocity improves end-to-end system performance. One of the issues that arises in connection with the use of power amplifiers, is non-linear clipping noise. To maintain

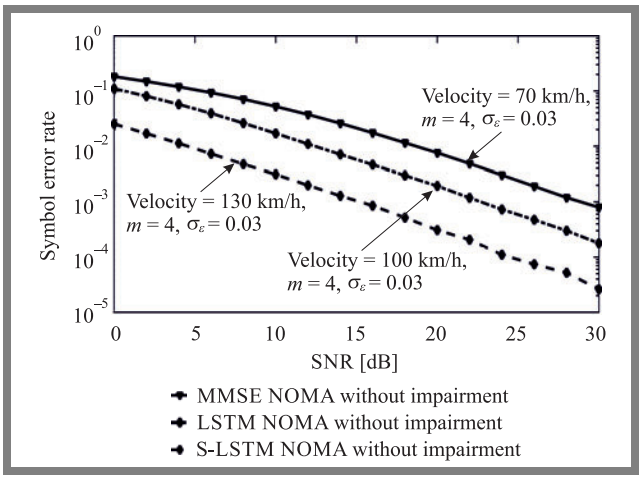

Fig. 16. SER vs. SNR plots considering all impairments for time-selective Nakagami-m fading connections.

the linearity of the power amplifier, the envelope cancellation scheme is used in this work. In Fig. 16, end-to-end error performance comparisons have been provided between the S-LSTM, MMSE and conventional NOMA receivers, considering BPSK modulated symbols. The S-LSTM NOMA detector has been found to perform better overall than the traditional SIC-based NOMA receiver when the clipping ratio is equal to two and the SNR is more than 14 dB. As shown in Fig. 17, performance improves significantly when S-LSTM is used, but the end-to-end system performance improves with a decrease in node velocity.

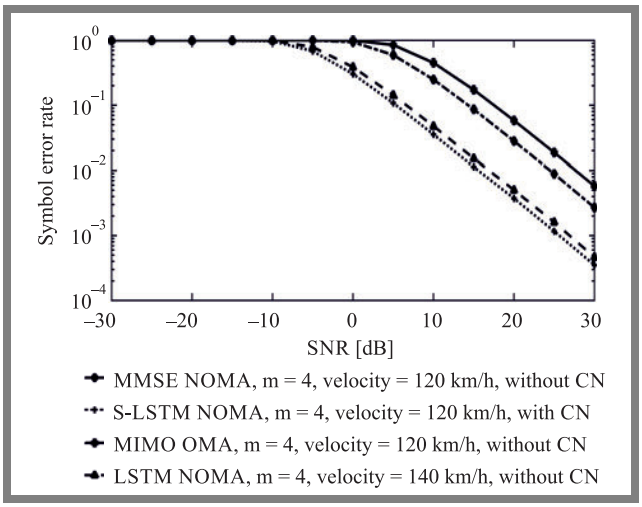

Fig. 17. Performance comparison between S-LSTM NOMA and other conventional NOMA schemes for various CP.

The time-varying fading channel coefficients in the online phase, considering BPSK symbols, are calculated using offline data sets. Performance difference between the offline and online states is shown in time-selective fading. Furthermore, these differences must be stable for the trained model. Figure 18 presents the results of the effect that is caused by changing the fading relationship statistics that are used during the training and testing stages. It is easy to understand that the performance of SER will improve if the number of

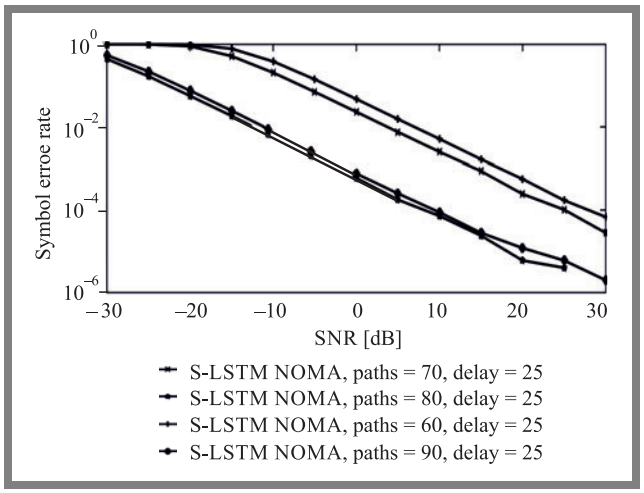

Fig. 18. Performance S-LSTM NOMA for various number of paths and delays with node velocity equal to 120 km/h.

possible paths is increased while maintaining the same fixed propagation delay.

5.3. Impact of Training Rate and Packet Length

The achievable data rate plots for VN_S are demonstrated in Fig. 19, along with an investigation for the S-LSTM MIMO-NOMA receiver trained at various training rates. It is evident that a lower training rate leads to a greater data transmission rate, supporting the hypothesis that a higher training rate would result in more frequent weight changes and a bigger validation error. A lower training rate of 0.004 improves accuracy, but slows down convergence, since more updates are required.

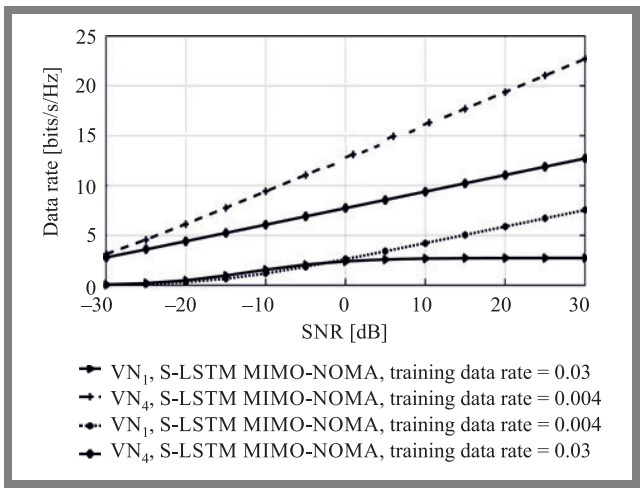

Fig. 19. Achievable data rates for various training data rates, considering node mobility equal to 120 km/h and error variance of $\sigma_\epsilon^2 = 0.02$.

To balance training accuracy and duration, the training rate has been adjusted to 0.03 for all other simulation scenarios. Smaller packets, however, offer reduced testing precision. Figure 20 shows the data rate that is achievable for different packet lengths when the node mobility is set to 130 km/h and the error variance is set to $\sigma_\epsilon^2 = 0.02$. Additionally, more data is used to offer a more precise estimate of the gradient for

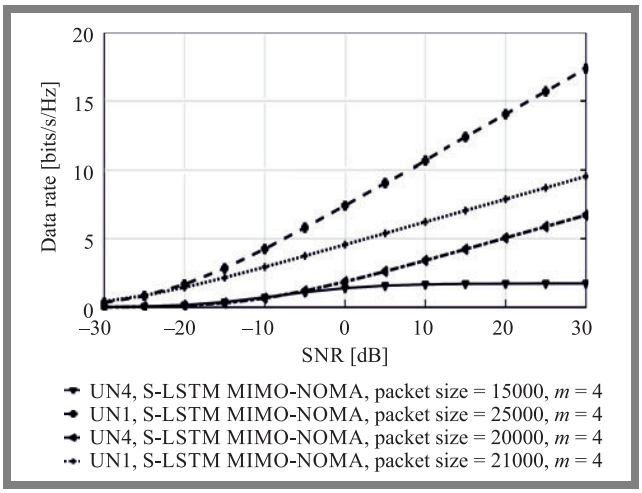

Fig. 20. Achievable data rate for various packet lengths, considering node mobility equal to 130 km/h.

each update, even though larger-sized packets require fewer iterations and updates of S-LSTM's parameters. Therefore, a final receiver with superior performance benefits from larger packet sizes.

6. Conclusion

This work presents a preliminary analysis of an S-LSTM-based MIMO-NOMA receiver and considers node mobility, SIC error and channel estimation error. Relative velocity between the BS and mobile users yields the ISI and time selectivity results in the enhanced end-to-end SER increase and OP. The simulation results show that the S-LSTM technique works better than the conventional SIC receiver and is more resistant to limited radio resources, such as SE, energy efficiency, number of pilot symbols, training rate, packet length, and CP than previous channel estimation methodologies. For more complex models, such as S-LSTM MIMO-NOMA systems, more research and testing will be performed. The entire training and testing procedure presented in this work starts with a time-selective channel profile. The impacts of node mobility and imperfect CSI will be examined for use in actual applications, in order to further evaluate the S-LSTM NOMA model's resistance to random channel profiles.

References

[1] M.H. Eiza, *et al.*, "Investigation of routing reliability of vehicular ad hoc networks", *J. Wireless Com Network.*, vol. 179, 2013 (DOI: 10.1186/1687-1499-2013-179).

[2] E.U. Ogbodo, E. Utochukwu, A.M. Abu-Mahfouz, and A.M. Kurien, "A Survey on 5G and LPWAN-IoT for Improved Smart Cities and Remote Area Applications: From the Aspect of Architecture and Security", *Sensors*, vol. 22, pp. 6313, no. 16, 2022 (URL: https://www.mdpi.com/1424-8220/22/16/6313/htm).

[3] Q. Qiu, D. Wang, X. Du, S. Yu, S. Liu, and B. Zhao, "Security standards and measures for massive IoT in the 5G era", *Mobile Networks and Applications*, vol. 27, no. 1, pp. 392–403, 2022 (DOI: 10.1007/s11036-021-01841-2).

[4] M. Verma, J. Sheetlani, V. Mishra, and M. Mishra, "An Integrated Technique for Security of Cellular 5G-IoT Network Healthcare Ar-

chitecture", *G. Ranganathan, R. Bestak R. Palanisamy, Á. Rocha, Pervasive Computing and Social Networking, Lecture Notes in Networks and Systems*, vol. 317, pp. 549–563, Singapore, 2022 (DOI: 10.1007/978-981-16-5640-8_42).

[5] T. Xu, C. Xu, and Z. Xu, "An efficient three-factor privacy-preserving authentication and key agreement protocol for vehicular ad-hoc network", *China Communications*, vol. 18, no. 12, pp. 315–331, 2021 (DOI: 10.23919/JCC.2021.12.020).

[6] H. Badis and A. Rachedi, "Modeling tools to evaluate the performance of wireless multi-hop networks", ed.: Mohammad S. Obaidat, Petros Nicopolitidis, Faouzi Zarai, *Modeling and Simulation of Computer Networks and Systems, Morgan Kaufmann*, pp. 653–682, ISBN 9780128008874, 2015 (DOI: 10.1016/B978-0-12-800887-4.00023-7).

[7] R. Tiwari and S. Deshmukh, "Analysis and design of an efficient handoff management strategy via velocity estimation in HetNets", *Transactions on Emerging Telecommunications Technologies*, vol. 33, no. 3, pp. e3642, 2022 (DOI: 10.1002/ett.3642).

[8] R. Tiwari and S. Deshmukh. "Prior information-based Bayesian MMSE estimation of velocity in HetNets", *IEEE Wireless Communications Letters*, vol. 8, no. 1, pp. 81–84, 2018 (DOI: 10.1109/LWC.2018.2857805).

[9] R. Tiwari and S. Deshmukh, "MVU estimate of user velocity via gamma distributed handover count in HetNets", *IEEE Communications Letters*, vol. 23, no. 3, pp. 482–485, 2019 (DOI: 10.1109/LCOMM.2019.2892962).

[10] D.K. Patel, *et al.*, "Performance Analysis of NOMA in Vehicular Communications Over i.n.i.d. Nakagami-m Fading Channels", *IEEE Transactions on Wireless Communications*, vol. 20, no. 10, pp. 6254–6268, Oct. 2021 (DOI: 10.1109/TWC.2021.3073050).

[11] H. Ahmad, D.M. Ali, W.N.W. Muhamad, and M.S. Idris, "Performance analysis of NOMA in pedestrian and vehicular environments", *Journal of Physics: Conference Series, IOP Publishing*, vol. 1502, no. 1, pp. 012003, 2020 (DOI: 10.1088/1742-6596/1502/1/012003).

[12] B.P. Chaudhary, R. Shankar, and R.K. Mishra, "A tutorial on cooperative non-orthogonal multiple access networks", *The Journal of Defense Modeling and Simulation*, vol. 19, no. 4, pp. 563–573, 2022 (DOI: 10.1177/1548512920986627).

[13] M.K. Beuria, R. Shankar, and S.S. Singh, "Analysis of the energy harvesting non-orthogonal multiple access technique for defense applications over Rayleigh fading channel conditions", *The Journal of Defense Modeling and Simulation*, vol. 19, no. 4, pp. 821–828, 2022 (DOI: 10.1177/15485129211021168).

[14] R. Malladi, M.K. Beuria, R. Shankar, and S.S. Singh, "Investigation of the fifth generation non-orthogonal multiple access technique for defense applications using deep learning", *The Journal of Defense Modeling and Simulation*, 2021 (DOI: 10.1177/15485129211022857).

[15] R. Shankar, T.V. Ramana, P. Singh, S. Gupta, and H. Mehraj, "Examination of the Non-Orthogonal Multiple Access System Using Long Short Memory Based Deep Neural Network", *Journal of Mobile Multimedia*, pp. 451–474, 2021 (DOI: 10.13052/jmm1550-4646.18214).

[16] R. Shankar, *et al.*, "Examination of user pairing NOMA system considering the DQN scheme over time-varying fading channel conditions", *Journal of Information Science and Engineering*, vol. 38, no. 4, 2022 (DOI: 10.6688/JISE.202207 38(4).0010).

[17] L. Chouhan, P.K. Sharma, and N. Varshney, "Optimal Transmitted Molecules and Decision Threshold for Drift-Induced Diffusive Molecular Channel With Mobile Nanomachines", *IEEE Transactions on NanoBioscience*, vol. 18, no. 4, pp. 651–660, 2019 (DOI: 10.1109/TNB.2019.2935241).

[18] Y. Sun, D.W.K. Ng, Z. Ding, and R. Schober, "Optimal joint power and subcarrier allocation for full-duplex multicarrier non-orthogonal multiple access systems", *IEEE Tran. Commun.*, vol. 65, no. 3, pp. 1077–1091, 2017 (DOI: 10.1109/TCOMM.2017.2650992).

[19] M. Choi, J. Kim, and J. Moon, "Dynamic power allocation and user scheduling for power-efficient and delay-constrained multiple access networks", *IEEE Trans. Wireless Commun.*, pp. 1–1, 2019 (DOI: 10.1109/TWC.2019.2929809).

[20] Z. Xiao, L. Zhu, J. Choi, P. Xia, and X. Xia, "Joint power allocation and beamforming for non-orthogonal multiple access (NOMA) in 5G millimeter wave communications", *IEEE Trans. Wireless Commun*, vol. 17, no. 5, pp. 2961–2974, 2018 (DOI: 10.1109/TWC.2018.2804953).

[21] B. Soni, D.K. Patel, Y.L. Guan, S. Sun, Y. C. Chang, and J. M-Y. Lim, "Performance Analysis of NOMA aided Cooperative Relaying over α-η-κ-μ Fading Channels", *National Conference on Communications (NCC)*, pp. 1–6, 2020 (DOI: 10.1109/NCC48643.2020.9056034).

[22] J. Men, J. Ge, and C. Zhang, "Performance analysis of non-orthogonal multiple access for relaying networks over Nakagami-m fading channels", *IEEE Trans. Veh. Technol.*, vol. 66, no. 2, pp. 1200–1208, 2017 (DOI: 10.1109/TVT.2016.2555399).

[23] J. Men, J. Ge, and C. Zhang, "Performance analysis for downlink relaying aided non-orthogonal multiple access networks with imperfect CSI over Nakagami-m fading", *IEEE Access*, vol. 5, pp. 998–1004, 2017 (DOI: 10.1109/ACCESS.2016.2631482).

[24] Y. Dursun, F. Fang, and Z. Ding, "Hybrid NOMA based MIMO offloading for mobile edge computing in 6G networks", *China Communications*, vol. 19, no. 10, pp. 12–20, 2022 (DOI: 10.23919/JCC.2022.00.024).

[25] Y. Dursun, K. Wang, and Z. Ding, "Secrecy sum rate maximization for a MIMO-NOMA uplink transmission in 6G networks", *Physical Communication*, vol. 53, pp. 101675, 2022 (DOI: 10.1016/j.phycom.2022.101675).

[26] D. Wan, M. Wen, F. Ji, Y. Liu, and Y. Huang, "Cooperative NOMA systems with partial channel state information over Nakagami-m fading channels", *IEEE Trans. Commun.*, vol. 66, no. 3, pp. 947–958, 2017 (DOI: 10.1109/TCOMM.2017.2772273).

[27] K-H. Nguyen, H.V. Nguyen, V-P. Bui, and O-S. Shin, "Dynamic User Pairing for Non-Orthogonal Multiple Access in Downlink Networks", *2020 IEEE Eighth International Conference on Communications and Electronics (ICCE)*, pp. 111–114, 2021 (DOI: 10.1109/ICCE48956.2021.9352141).

[28] H. Ye, G.Y. Li, and B. Juang, "Power of deep learning for channel estimation and signal detection in OFDM systems", *IEEE Wireless Communications Letters*, vol. 7, 2018 (DOI: 10.1109/LWC.2017.2757490).

[29] N. David, U. Wolfgang, and W. Thomas, "Deep channel estimation", *Proc. 21st International ITG Workshop on Smart Antennas*, 2017.

[30] M. Vaezi, R. Schober, Z. Ding, and H.V. Poor, "Nonorthogonal Multiple Access: Common Myths and Critical Questions", *IEEE Wireless Communications Magazine*, vol. 26, no. 5, 2019 (DOI: 10.1109/MWC.2019.1800598).

[31] G. Gui, H. Huang, Y. Song, and H. Sar, "Deep Learning for an Effective Non-orthogonal Multiple Access Scheme", *IEEE Transactions on Vehicular Technology*, vol. 67, no. 9, 2018 (DOI: 10.1109/TVT.2018.2848294).

[32] J-M. Kang, I-M. Kim, and C-J. Chun, "Deep Learning-Based MIMO-NOMA With Imperfect SIC Decoding", *IEEE Systems Journal*, vol. 14, no. 3, pp. 3414–3417, 2020 (DOI: 10.1109/JSYST.2019.2937463).

[33] J. Pan, N. Ye, A. Wang, and X. Li, "A Deep Learning-Aided Detection Method for FTN-Based NOMA", *Hindawi Wireless Communications and Mobile Computing*, vol. 2020, 2020 (DOI: 10.1155/2020/5684851).

[34] L. Chuan, C. Qing, and L. Xianxu, "Uplink NOMA signal transmission with convolutional neural networks approach", *Journal of Systems Engineering and Electronics*, vol. 31, 2020 (DOI: 10.23919/JSEE.2020.000068).

[35] M.A. Aref and S.K. Jayaweera, "Deep Learning-aided Successive Interference Cancellation for MIMO-NOMA", *IEEE Global Communications Conference*, pp. 1–5, 2020 (DOI: 10.1109/GLOBECOM42002.2020.9348107).

[36] R. He, A.F. Molisch, F. Tufvesson, Z. Zhong, B. Ai, and T. Zhang, "Vehicle-to-vehicle propagation models with large vehicle obstructions", *IEEE Trans. Intell. Transp. Syst.*, vol. 15, no. 5, pp. 2237–2248, 2014 (DOI: 10.1109/TITS.2014.2311514).

[37] M. Alouini and A.J. Goldsmith, "A unified approach for calculating error rates of linearly modulated signals over generalized fading channels", *IEEE Trans. Commun.*, vol. 47, no. 9, pp. 1324–1334, 1999 (DOI: 10.1109/26.789668).

[38] D. Kalita, "An Overview on Long Short Term Memory (LSTM)", (URL: https://www.analyticsvidhya.com/blog/2022/03/an-overview-on-long-short-term-memory-lstm/).

[39] –, "Long Short-Term Memory Networks", (URL: https://in.mathworks.com/help/deeplearning/ug/long-short-term-memory-networks.html).
[40] R. Shankar and R.K. Mishra, "PEP and OP examination of relaying network over time-selective fading channel", *SN Appl. Sci.*, vol. 2, pp. 1329, 2020 (DOI: 10.1007/s42452–020–3077–5).
[41] C.B. Barneto *et al.*, "Full-duplex OFDM radar with LTE and 5G NR waveforms: Challenges, solutions, and measurements", *IEEE Transactions on Microwave Theory and Techniques*, vol. 67, no. 10 pp. 4042–4054, 2019 (DOI: 10.1109/TMTT.2019.2930510).
[42] R. Shankar and R.K. Mishra, "Investigation of multiple hop cooperative communication system over time-selective Nakagami-m fading channel", *Iran. J. Comput. Sci.*, vol. 3, pp. 145–168, 2020 (DOI: 10.1007/s42044-020-00054-2).
[43] C. Lin, Q. Changr, and X. Li, "A Deep Learning Approach for MIMO-NOMA Downlink Signal Detection", *Sensors*, vol. 19, no. 11, pp. 2526, 2019 (DOI: 10.3390/s19112526).
[44] K.M. Deep, "Learning SIC Approach for Uplink MIMO-NOMA System", *University of Oulu, Faculty of Information Technology and Electrical Engineering, Degree Programme in Wireless Communications Engineering, Master's thesis*, 50, p. 2022 (URL: http://jultika.oulu.fi/files/nbnfioulu-202208163315.pdf).
[45] Z. Wei, D.W.K. Ng, and J. Yuan, "Joint Pilot and Payload Power Control for Uplink MIMO-NOMA With MRC-SIC Receivers", *IEEE Communications Letters*, vol. 22, no. 4, pp. 692–695, 2018 (DOI: 10.1109/LCOMM.2018.2798658).
[46] Z. Wei, L. Yang, D. W. K. Ng, and J. Yuan, "On the Performance Gain of NOMA over OMA in Uplink Single-Cell Systems", *2018 IEEE Global Communications Conference*, pp. 1–7, 2018 (DOI: 10.1109/GLOCOM.2018.8647743).
[47] Z. Wei, D.W. Ng, and J. Yuan, "Joint Pilot and Payload Power Control for Uplink MIMO-NOMA with MRC-SIC Receivers", *IEEE Communications Letters*, vol. 22, no. 4, 2018 (DOI: 10.1109/LCOMM.2018.2798658).
[48] D. Di Caprio and F.J. Santos-Arteaga, "Enhancing the pattern recognition capacity of machine learning techniques: The importance of feature positioning", *Machine Learning with Applications*, vol. 7, pp. 100196, 2022 (DOI: 10.1016/j.mlwa.2021.100196).
[49] V. Andiappan and V. Ponnusamy, "Deep Learning Enhanced NOMA System: A Survey on Future Scope and Challenges", *Wireless Pers. Commun.*, vol. 123, pp. 839–877, 2022 (DOI: 10.1007/s11277-021-09160-1).
[50] Narengerile and J. Thompson, "Deep Learning for Signal Detection in Non-Orthogonal Multiple Access Wireless Systems", *UK/China Emerging Technologies (UCET)*, pp. 1–4, 2019 (DOI: 10.1109/UCET.2019.8881888).
[51] Narengerile, "Deep learning for signal detection in NOMA", *MATLAB Central File Exchange*, 2022 (URL: https://www.mathworks.com/matlabcentral/fileexchange/75478-deep-learning-for-signal-detection-in-noma-systems).
[52] X. Du, H. Zhang, H.V. Nguyen, and Z. Han, "Stacked LSTM Deep Learning Model for Traffic Prediction in Vehicle-to-Vehicle Communication", *IEEE 86th Vehicular Technology Conference (VTC-Fall)*, pp. 1–5, 2017 (DOI: 10.1109/VTCFall.2017.8288312).
[53] J. Brownlee, "Stacked Long Short-Term Memory Networks", (URL: https://machinelearningmastery.com/stacked-long-short-term-memory-networks/).

Ravi Shankar received his B.E. degree in Electronics and Communication Engineering from Jiwaji University, India, in 2006. He received his M. Tech. degree in Electronics and Communication Engineering from GGSIPU, India, in 2012. He received a Ph.D. in Wireless Communication from the National Institute of Technology Patna, in 2019. He was an Assistant Professor at MRCE Faridabad, from 2013 to 2014, where he was engaged in researching wireless communication networks. He is presently an Assistant Professor at SR University, Warangal, India. His current research interests cover cooperative communication, D2D communication, IoT/M2M networks and network protocols.

https://orcid.org/0000-0001-7532-3275
E-mail: ravi.mrce@gmail.com
Electronics and Communication Engineering Department, SR University, India

Bhanu Pratap Chaudhary is working as Research Scholar at National Institute of Technology Patna in Electronics and Communication Engineering department. He received his M. Tech. degree in Microelectronics & amp, VLSI design from National Institute of Technology, India. He received his B.Tech. degree in Electronics & Communication Engineering from CET-IILM-AHL, India. He is presently an Assistant Professor at Manav Rachna International Institute of Research and Studies, India. His current research interests cover cooperative communication, D2D communication, IoT/M2M networks and network protocols.

https://orcid.org/0000-0001-7085-4130
E-mail: bhanuc.phd18.ec@nitp.ac.in
Electronics and Communication Engineering Department, National Institute of Technology Patna, India

Ritesh Kumar Mishra received his B.E. degree in Electronics and Communication Engineering from Shivaji University, India, in 1998. He received his M.Tech. degree in Electronics and Communication Engineering from University of Burdwan, WB, India, in 2004. He received his Ph.D. in Wireless Communication from LNMU, Bihar, India, in 2011. He is presently working as an Assistant Professor at the National Institute of Technology Patna, Patna, India and has been engaged in researching wireless communication networks. His current research interests focus on cooperative communication, D2D communication, IoT/M2M networks.

https://orcid.org/0000-0002-7996-2231
E-mail: ritesh@nitp.ac.in
Electronics and Communication Engineering Department, National Institute of Technology Patna, India